Hybrid PVT solar systems optimization for household applications
Extended abstract

Miguel Carneiro (n.73635)

A model that describes a Photovoltaic/Thermal (PVT) solar system at the domestic sector was developed, simulated and its investment costs optimized through Genetic Algorithms.

The model consists of a combination of solar irradiance estimations with the development and simulation of a PV+PVT array for domestic hot water heating (DHW). It also includes a climatization system that incorporates a heat pump, an inertial water tank (IT) for energy storage and convective fans for air conditioning. Defining the building's construction and location, the framework for its heating/cooling needs and the DHW and electricity consumption profiles of its occupants, the model's optimization process is able to predict the different system's properties that minimize the investment costs while maintaining the household needs fulfilled.

Two optimization case studies, S1 and S2, are presented for a residential unit in Lisbon. In S1, the available area is limited do 30 m^2 and the excessive PV generation is sold to the grid. A Levelized Cost of Energy (LCoE) of 0.136 EUR/kWh and a payback time of 7.9 years were determined. In S2, considering an unlimited area and the excessive PV generation's loss, the LCoE was 0.148 EUR/kWh with a payback time of 8.7 years. A PV area of 22.4 m^2 and PVT area of 7.1 m^2 provided 54.7 % of the household's electrical and 78.2 % of its thermal demand.

I. INTRODUCTION

Cogeneration systems (*Combined Heat and Power* - CHP) are broadly defined as the coincident or simultaneous generation of the combined heat and power by sequential use of energy from one primary energy source. As a result of the electricity production CHP allows the conversion of excessive heat into useful energy. In CHP the energy conversion efficiency can reach almost 80% in comparison to the 30–35% efficiency of typical fossil fuel fired power plants [1]. In such systems, fossil fuels are still the main energy source while biomass[2], thermoelectric [3] and Photovoltaic/Thermal hybrid systems escape these traditional energy sources, much needed in order to fulfill the current worldwide energy policies and needs [4]. Even though Photovoltaic (PV) systems have been in the market for several years as a commercially reliable alternative method to fossil fuel based electricity production, there are still challenges to overcome regarding such applications. Challenges such as elevated cell temperatures, limited electrical conversion efficiency and dust accumulation severely impact PV performance. E. Radziemska [5] experimentally measured this temperature influence between 28 °C and 80°C in a crystalline silicon cell. A 0.65%/K decrease in the output power, a *Fill Factor's* decrease of 0.2%/K and a 0.08%/K decrease in the conversion efficiency were measured. Therefore, preventing the cell from reaching very high temperatures is crucial for an optimal PV performance, while avoiding long term degradation of the system [6].

By combining the generation of both electrical and thermal energy, Photovoltaic/Thermal (PVT) systems increase the overall efficiency per unit area in comparison with isolated PV modules and solar collectors. Moving energy generation closer to point of use point of use, has obvious benefits on a residential's energy independence, making these systems particularly promising for domestic applications [9][10][11].

$$\begin{bmatrix} I_1 \\ I_2 \\ \vdots \\ I_n \end{bmatrix} = \begin{bmatrix} c_{11} & c_{12} & c_{13} & \dots & c_{1j} \\ c_{21} & c_{22} & c_{23} & \dots & c_{2j} \\ \vdots & \vdots & \vdots & \ddots & \vdots \\ c_{n1} & c_{n2} & c_{n3} & \dots & c_{nj} \end{bmatrix}$$

Figure 1: A matricial representation of a population P(t) in GA

II. GENETIC ALGORITHMS IN PVT SYSTEMS

The individuals of a population in a Genetic Algorithm (GA) represent the solutions space and each individual is described by a set of the system's variables. The GA starts, then, by randomly generating an initial population, P(t = 0). The population P(t) of n individuals interacts with an environment which returns a respective fitness f_1, ..., f_n. To each individual I_1,...,I_n there is a corresponding chromosome c_{11},...,c_{nj} that encodes the individual's genetic information, as Figure II shows, which, in this case, represents the total optimized variables j from the modeled system.

The evolutionary process of GA from a population P(t) to P(t+1) contemplates the processes of *selection*, *crossover*, and *mutation*. The *selection* operation selects parents according based on some relative fitness criterion. An individual can be selected more than once as a parent, in which case it contributes its genes to more than one child. The *crossover* operation takes pairs of selected parents and allows them to produce children containing their genetic information. The *mutation* operation changes some random portion of the chromosome of an individual. Successive generations will produce in-

creasingly fit individuals.

A ranking function that sorts the probability of selection according to an individual's fitness is required. The Fitness Scaling option *Rank*, scales the raw fitness scores based on the rank of each individual which is its position in the sorted scores, being 1 the most fit individual, 2, the next most fit and so on. The scaled score is proportional to $1/\sqrt{r}$, where r is the individual's rank. So the scaled score of the most fit individual is proportional to 1, the scaled score of the next most fit is proportional to $1/\sqrt{2}$, etc. Because the algorithm minimizes the fitness function, lower raw scores have higher scaled values. Another fitness scaling function can be *Fitness Scaling Top* which scales the individuals with the higher fitness function equally and the remaining with 0. The percentage of the population that integrates the best and worst fitted can be defined.

The selected option goes from *Tournament*, *Roullette wheel* to the *Stochastic uniform* The *Stochastic uniform* lays out a line in which each parent corresponds to a section of the line of length proportional to its scaled value. The algorithm moves along the line in steps of equal size. At each step, the algorithm allocates a parent from the section it lands on. The *Tournament* selection chooses a parent by assigning it to the individual with the highest scaled value over 4 individuals randomly selected.

As it iterates to the next generation, P(t+1), the GA creates three types of children: *Elite children* are the individuals with the best fitness values. These individuals automatically survive to the next generation and it can be specified the amount that are guaranteed to survive, *Crossover children* are created by combining the vectors of a pair of parents and *Mutation children* are created by introducing random changes, or mutations, to a single parent.

The Crossover fraction specifies the fraction of each population, other than elite children, that is made from crossover children. A crossover fraction of 1 means that all children other than elite individuals are crossover children, while a crossover fraction of 0 means that all children are mutation children. Neither of these extremes is an effective strategy for optimizing a function. The method of crossover can also be specified.

The GA is interrupted if a stopping criteria is met. This can vary from the average relative change in the best fitness function value when lower than a defined tolerance, converging, then, to a local minimum, to a maximum number of generations allowed.

III. FINANCIAL ANALYSIS

The integration's liability mainly depends on the initial investment costs and its payback time. The payback time value is the year in which the Net Present Value (NPV) is zero, following

$$\text{NPV} = \sum_{y=1}^{y} \frac{\text{Solar Savings}}{(1+dr)^y} - C_0, \tag{1}$$

where C_0 is the total investment costs, dr is the discount rate, y the current year and the levelized cost of energy (LCoE) is given by

$$\text{LCoE} = \frac{C_E + C_0}{E_{demand}}, \tag{2}$$

in an annual basis balance. C_E is the the annual balance between the energy expenses with electricity and the energy sales to the grid and E_{demand} the energy demand for the same period.

The system's lifetime was held over a 20 year period which included a single PV+PVT array and two DHW and IT tanks throughout that time. The investment costs also include the maintenance costs. These were considered to be 1% of the investment for each element that comprises the calculated costs. The main goal of this work is, then, to present reliable tool that determines the minimum $C_E + C_0$ that sustains the system's operation for its lifetime period, while complying with the residential's needs.

IV. THE SYSTEM

A. PVT + PV + DHW

The PVT thermal efficiency in steady state conditions is given by

$$\eta_{th} = \frac{\dot{m}_{PVT}\, c_{p,w}(T_{fo} - T_{fi})}{A_{PVT} G_T}, \tag{3}$$

where T_{fo} and T_{fi} are the PVT collector outlet and inlet temperatures, $\dot{m}_{PVT}$ the mass flow rate at the collector, A_{PVT} the PVT area, G_T the incident irradiance on the module and $c_{p,w}$ the water's specific heat.

J. H. Kim and J. T. Kim [12] experimentally compared the electrical and thermal performances of glazed and unglazed PVT collectors. Its correlations are used in this work in order to calculate the electrical and thermal efficiencies as a function of $\Delta T = T_{fi} - T_a$. The thermal and electrical efficiencies, η_{th} and η_{elec}, can be expressed as

$$\eta_{th,elec} = \eta_0 - U_{PVT,th,elec} \frac{\Delta T}{G_T}. \tag{4}$$

The heat gain from the PVT is given by

$$\dot{Q}_{PVT} = \eta_{th} G_T\, A_{PVT}. \tag{5}$$

An inverter to convert the PVT's DC output to an AC transmission deliverable to the network is required and part of the system. The electrical energy rate output by the PVT is given by

$$\dot{E}_{elec} = \eta_{elec}\, G_T\, A_{PVT}\, \eta_{inv}, \tag{6}$$

where η_{inv} is the inverter efficiency, which includes the Maximum Power Point Tracking (MPPT) efficiency.

The DHW storage tank thermal balance equation is given by

$$\begin{aligned} M_{DHW}\, c_{p,w}\, \frac{dT_{DHW}}{dt} &= \eta_{th} G_T A_{PVT} \\ -\dot{m} c_{p,w} (T_{DHW} - T_{main}) &\\ + UA_{DHW}\, (T_{house} - T_{DHW}). & \end{aligned} \tag{7}$$

with γ_{DHW} being the DHW thermostat that limits the maximum DHW temperature and $\gamma_{DHW,2}$ that is responsible for preventing the tank going below a minimum DHW temperature.

In a stand-alone PV system, the module's operating temperature is [13]

$$T_{PV} = \frac{G_T}{800}(\mathrm{NOCT} - 20) + T_a. \tag{8}$$

The Nominal Operating Cell Temperature (NOCT) is defined as the mean solar cell junction temperature within an open-rack mounted module under open-circuit conditions operating in a nominal terrestrial environment (NTE), that is: tilt angle at normal incidence to the direct solar beam at local solar noon; incident irradiance of 800 W/m^2; ambient temperature, T_a, of 20 °C and wind speed of 1 m/s. [14][15]

The linear correlation regarding the PV electrical efficiency is given by Evans–Florschuetz

$$\eta_{elec} = \eta_{ref}\Big[1 - \beta_{ref}(T_{m,PV} - T_{ref})\Big], \tag{9}$$

in which η_{ref} is the module's electrical efficiency at the reference temperature, T_{ref}, and at solar radiation flux of 1000 W/m^2. The temperature coefficient, β_{ref}, is a property of the crystalline silicon modules given by the manufacturer and T_{PV} the cell's/module operating temperature from Equation 8 [15].

B. Radiation Model

It is necessary to estimate the irradiance on the PVT's surface, I_T. In order to accomplish it, this work follows the Perez et al. [16] anisotropic sky model which, as opposed to the isotropic sky model that underestimates the total incident radiation, it takes into account the circumsolar and horizon brightening components of diffuse radiation with increased accuracy adding the circumsolar and horizon brightening coefficients F_1 and F_2. The total hourly irradiance on the tilted surface is given by

$$\begin{aligned} I_T = I_b\, R_b + I_d\,(1 - F_1)\,\frac{1 + \cos\beta}{2} + I_d\, F_1\, \frac{a}{b} & \\ + I_d\, F_2\, \sin\beta + I\, \rho\, \frac{1 - \cos\beta}{2}, & \end{aligned} \tag{10}$$

where I_b is the beam component on a horizontal surface, I_d the diffused component and I the estimated or measured total irradiation for the considered time interval on a horizontal surface, being $I = I_b + I_d$. The factors a and b are given as $a = \max(0,\ \cos\theta)$, $b = \max(\cos 85°,\ \cos\theta_z)$ and ρ is the ground's reflectance coefficient (albedo). The brightness coefficients F_1 and F_2 are functions of three parameters that describe the sky conditions, which are the zenith angle θ_z, a clearness parameter ϵ, and a brightness parameter Δ. The parameter ϵ is a function of the hour's diffuse radiation I_d and normal incidence beam radiation $I_{b,n} = I_b / \cos\theta_z$.

However, to proceed with the anisotropic sky model of Perez et al. an estimation of the distribution between beam and diffused radiation is necessary. Studies on available data allow a correlation of the diffused fraction, I_d/I, with the clearness index k_T, the ratio between the total irradiance incident on the horizontal surface, I, and its predicted pre-atmospheric I_o irradiance. This work follows the Erbs et al. correlation [17] from available radiation data from US and Australian stations.

$$\frac{I_d}{I_o} = \begin{cases} 1\text{–}0.09\, k_T, & k_T \le 0.22 \\ 0.9511 - 0.1604\, k_T + 4.388\, k_T^2 - 16.638\, k_T^3 + 12.336\, k_T^4, & 0.22 < k_T \le 0.80 \\ 0.165, & k_T > 0.80 \end{cases} \tag{11}$$

C. Heat Pump/Chiller

A Heat pump transfers heat from a low temperature, or cold, source to a high temperature, or hot, source. According to the second law of thermodynamics, such system demands an expenditure of energy, a thermody-

namic input, in the form of work. The vapor compression heat pump is the most common variant that requires a work input through a mechanical compressor, typically driven by an electric motor, that leads the heat transfer fluid a from a low temperature state to a high temperature state. This kind of heat pumps are widely used for residential and commercial heating and cooling, this work's object of study [18].

Taking a heat pump operating within a house with the heating mode, as an example, the cold source, or the evaporator, would be the ambient air and the hot source, or the condenser, the circulating water at the heat pump for subsequent heat exchange with the house's inside air. For the cooling mode, heat flows in the opposite direction.

Thus, the measure of performance is given by the fraction between the useful heat and the system's work input. For the heat pump, the coefficient of performance (COP) is calculated with Q_H as the useful heat,

$$COP_{HP} = \frac{Q_H}{W} \tag{12}$$

and for the chiller the energy efficiency ratio is calculated with Q_L as the useful heat

$$EER = \frac{Q_L}{W} \tag{13}$$

The heat transfered from the condenser to the circulating water can be expressed, in steady-state conditions, as

$$\dot{Q}_H = \dot{m}_{HP}\, c_{w,p}(T_{fo} - T_{fi}), \tag{14}$$

in which T_{fo} and T_{fi} are the outlet and inlet water temperatures, respectively and $\dot{m}_{HP}$ the water flow rate.

D. Inertial Tank

The system also includes an inertial water tank (IT) for heat storage. These kind of vessels are often integrated in distributed energy systems for wasted heat recovering from a generation device, as CHP systems, using it for space or hot water heating. The tank is connected to the heat pump/chiller and to the convective fans in two separated closed water connections.

Assuming that the stored water's total mass remains constant over time, the water's pressure at the working temperatures is sufficiently high to prevent a water phase change, neglecting the radial temperature gradient and the heat exchanger's heat capacity, the energy transfer equations for a stratified tank model with N= 4 nodes including the energy flow to the convective fans, are given by

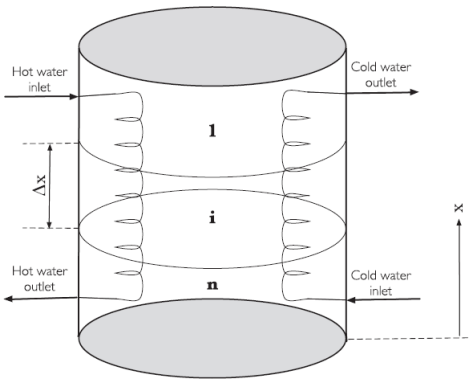

Figure 2: Inertial tank in thermal contact with the heat exchanger [19]

$$\begin{aligned} M_{strat} c_{p,w} \frac{dT_{IT,i}}{dt} &= r_i\, UA_{exch,i}(T_{exch,i} - T_{IT,i}) \\ &+\gamma_{CF}\, \dot{m}_{CF} c_{p,w}(T_{IT,i+1} - T_{IT,i}) \\ &+UA_{IT}(T_a - T_{IT,i}) \\ +\frac{\lambda_w\, A}{\Delta x}(T_{IT,i+1} - T_{IT,i}) &+ \frac{\lambda_w\, A}{\Delta x}(T_{IT,i-1} - T_{IT,i}). \end{aligned} \tag{15}$$

where Δx is the node's height, $T_{exch,i}$ the water temperature in the heat exchanger at the node i, $T_{CF,fo}$ the water temperature at the convective fans' output, entering the tank at the fourth node, λ_w is the water thermal conductivity and γ_{CF} is the command from the house's thermostat, alterning between 1 (ON state) and 0 (OFF state), connecting or disconnecting the water circulation at the convective fans ($\dot{m}_{CF}$). No node mixing was considered and all the calculations assume an immediate stratification as soon as the heat pump circulates water.

Since the heat transport from the circulating water at the heat exchanger and the stored water at the IT is a sum of the thermal resistances, the overall heat exchanger's heat transfer coefficient at the node i is

$$UA_{exch,i} = \frac{1}{\frac{1}{h_i\, S_i} + \frac{\ln(d_o/d_i)}{2\pi\, \lambda_{exch}\, \Delta x} + \frac{1}{h_o\, S_o}}, \tag{16}$$

with S_o and S_i being the outer and inner tube's section, h_o and h_i the outer and inner tube's heat transfer coefficient, respectively, at the node i and λ_{exch} the heat exchanger's thermal conductivity.

Following Rahman et al. [19] 1-D transient model for the heat transfer fluid (i.e. water inside the heat exchangers), the mass at the node i of the heat exchanger is considered stationary (transient heating) which becomes more valid as the number of equally divided number of nodes increases, leaving the energy balance equations at the heat exchanger level to be as

$$M_{exch,i}\, c_{p,w} \frac{dT_{exch,i}}{dt} = \gamma_{HP}\, \dot{m}_{HP}(T_{exch,\,i-1} - T_{exch,i}) + r_i\, UA_{exch,i}\,(T_{IT,i} - T_{exch,i}), \tag{17}$$

Therefore, taking from Equation 17, the mass $M_{exch,i}$ at the local node of the heat exchanger can be determined by

$$M_{exch,i} = \rho_w\, \pi\, (d_i/2)^2\, L_{exch,i}, \tag{18}$$

where $L_{exch,i}$ is the heat exchanger node length, d_i the inner tube diameter and r_i the heat exchanger length ratio over the node height.

The direct circulation approach describes a temperature stratification water tank's model that instead of including a heat exchanger, hot/cold water flowing from the heat pump circulates inside the stored water, exchanging heat without physical interfaces. Considering that energy must be conserved in a node, the energy balance equations that describe the heat flow at a node i are given by,

$$M_{strat}\, c_{p,w} \frac{dT_{IT,i}}{dt} = \gamma_{HP}\, \dot{m}_{HP} c_{p,w}(T_{IT,i-1} - T_{IT,i}) + \gamma_{CF}\, \dot{m}_{CF} c_{p,w}(T_{IT,i+1} - T_{IT,i}) + UA_{IT,i}(T_a - T_{IT,i}) + \frac{\lambda\, A}{dx}(T_{IT,i-1} - T_{IT,i}) + \frac{\lambda\, A}{dx}(T_{IT,i+1} - T_{IT,i}). \tag{19}$$

E. Convective fans

During the summer period, where cooling is needed, cold water leaves the inertial exchanging heat with air, circulating back to the tank with a higher temperature, while the opposite goes during the winter season.

Again disregarding the pipe's heat losses, the energy balance equation at the convective can be described as

$$\dot{m}_{CF}\, c_{p,w}(\, T_{CF,out} - T_{CF,in}) = UA_{CF}(T_{CF,in} - T_{room}). \tag{20}$$

where $T_{CF,fi} = T_{IT,1}$ is the temperature of the water that leaves the inertial tank at the top node, $T_{CF,fo}$ the temperature of the water that enters the at the bottom node, $\dot{m}_{CF}$ is the water's flow rate leaving the tank, $UA_{CF} = UA_{CF,1} + UA_{CF,2}$ the total heat transfer coefficient between the water and the air.

F. House

The building's room temperature, T_{room}, is given by,

$$M_{air}\, c_{p,a} \frac{dT_{room}}{dt} = UA_{wall,i}(T_{wall,i} - T_{room}) + UA_{roof,i}(T_{roof,i} - T_{room}) + UA_{windows}(T_a - T_{room}) + \gamma_{CF}\, UA_{CF}(T_{CF,in} - T_{room}) + \dot{m}_{inf}\, c_{p,a}(T_a - T_{room}) \tag{21}$$

where

$$T_{wall,i} = \frac{T_{room}\, UA_{wall,i} + T_{wall}\, UA_{wall} + G_{wall,i}}{UA_{wall} + UA_{wall,i}}, \tag{22}$$

$$T_{roof,i} = \frac{T_{room}\, UA_{roof,i} + T_{roof}\, UA_{roof}}{UA_{roof} + UA_{roof,i}} \tag{23}$$

with the i and o, subscripts indicating, in this case, the inside surface, closest to the room temperature, and outside surface, closest to the ambient temperature. The equations for T_{wall} and T_{roof} are analogous.

V. IMPLEMENTATION

A. Solar radiation validation

Figure 3 depicts a detailed comparison between available data and this model's estimation.

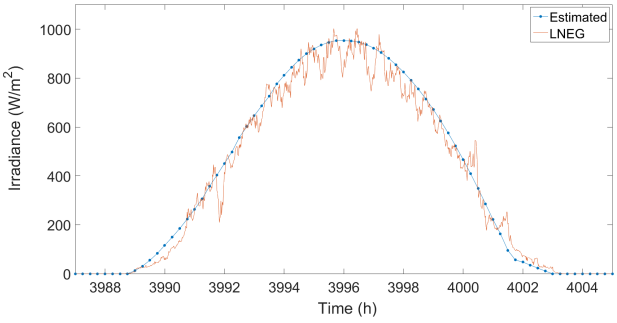

Figure 3: Detailed comparison between available data from *Laboratório Nacional de Energia e Geologia* (LNEG) and the model's estimation of G_T with $\beta = 38.7°$

In order to calculate the incident irradiance on a sloped surface, G_T, with $0° \leq \beta \leq 90°$ it is clear that the pre-

sented model is a valid tool.

B. Inertial Tank

For heat exchanging purposes, the tank's sectional area is necessary. To correlate the tank's dimensions with the specified volume, the data made available by the manufacturer was linearly interpolated with respect to the tank's diameter and height as shown in Figure 4.

For simulation purposes, it's, then, necessary to calculate U as a function of V. From experiment results on an IT of 1000 L, $U = 1.034 \pm 0.107$ W m^{-2} °C^{-1} and from the manufacturer's heat losses data the results were fit to a power expression of the type $f(x) = ax^b + c$. The fit outcome is shown in Figure 5.

The comparison between the model and simulation results with the experimental ones can be seen in Figure 6. The tank's temperature is considered to be uniform over a 1 m^3 of water storage, for this procedure. A constant input of around 7 kW heats the tank until it reaches the experimental temperature and from that moment the pulse generator interrupts the heat flux. That happens at $t = 4$ h. At that time, $T_{IT,simul}$ and $T_{IT,exper}$ are both at 40.9 °C. 14 hours later, at $t = 18$ h, the temperature difference between the two is of 0.5 °C, a 1.4 % deviation of the experimentally measured temperature.

C. Heat Pump/Chiller

The chiller's operating mode was fitted to a polynomial function from Carrier's manufacturer data. Figure 7-a) depicts the fitting results and the residuals at $T_a =$ 35 °C are plotted in Figure 7-b). The curve's behaviour seems to be in accordance with the expected with a Root Mean Square (RMS) of 0.07636. The entering water temperature at the chiller ranges between 9 - 23 °C.

For the heating mode, the fitting results that describe the COP as a function of $COP(T_{water,in}, T_a)$ are given in Figure 8.

D. House

As mentioned TRNSYS simulation software was used to estimate to a higher degree of certainty the real room temperature in a house with a typical portuguese construction, being then possible to determine UA for each interface [20]. At total, the residential area is 150 m^2 with a volume of 600 m^3, i.e., 15 x 10 m at the base and 4 m of height at the walls. The 60 m^2 walls are faced South and North, with one 3 m^2 window facing South and one other 2 m^2 window facing East, placed on a 40 m^2 wall. No interior divisions were designed. The results within a yearly time period can be seen in Figure 9, and the outcome of the different UA is visible in Table I. The subscript s represents the different surfaces $s =$ [wall, roof]. The windows overall heat transfer coefficient is $UA_{windows} = 7$ W °C^{-1}. The outer heat transfer coefficient that accounts for the convection between the air temperature and the outer wall and roof's surface layers was set to be 25 W m^{-2} °C^{-1} and the inside heat transfer coefficient that accounts for the convection between the room's temperature and the inside wall and roof's surface layers was set to be 7.7 W m^{-2} °C^{-1}.

This work's model does not fully account for internal radiative gains or the convective gains from the ground's surface neither its heat capacitance. A discrepancy in the thermal response amplitude for temperature changes is observable from Figure 9, where the TRNSYS simulation for the house's temperature, T_{TRNSYS}, is compared with this work's estimation, T_{house}, for a yearly time period. The instantaneous temperature difference reached between the two rarely exceeded 2 °C, with a differential maximum when close to the solar noon and before sunrise where the air temperature is at its highest and lowest, showing that this work's estimation is more susceptible to the ambient temperature.

Table I: Values for UA_s, with $s =$ [wall, roof] and its different components.

(W/ °C)	$UA_{s,o}$	UA_s	$UA_{s,i}$
Wall	240.90	248.51	1501.50
Roof	150.54	150.11	1155

VI. RESULTS - OPTIMIZATION

The optimization was conducted on the developed system with the *Direct Circulation approach*. For the sake of presenting case studies within this work's time window, this approach was selected since its computation time is 79 seconds for each individual, 5.62 times faster than the *Heat Exchanger approach*.

The system's optimized input variables that make up each individual's genetic code are displayed in Figure 10, where A_{PVT} and A_{PV} are the PVT and PV total area, respectively, V_{DHW} and V_{IT}, the DHW and IT tanks' volumes, respectively, $T_{DHWset,2}$, the DHW tank setpoint temperature that confines the tank within the setpoint region and $T_{ITset,w}$ and $T_{ITset,s}$, the IT temperature setpoint for the winter and summertime periods.

The GA options were a Stochastic Selection function, a Rank Fitness Scaling, a Population size of 200 individuals, Elite counting of 15, Crossover fraction of 0.9, Scattered Crossover function and Uniform Mutation. Two optimization scenarios were conceptualized and they're shown in Table II. Scenario S1 limits the PV+PVT area, finding which proportion of PV and PVT is optimal for 30 m^2 of available area. It also considers the excessive generation of electrical energy to be sold to the grid. On

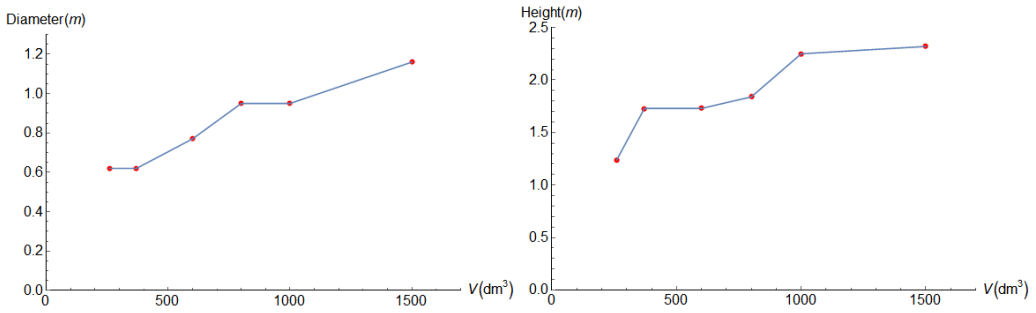

Figure 4: Linear interpolation of the tank's volume with its height and diameter

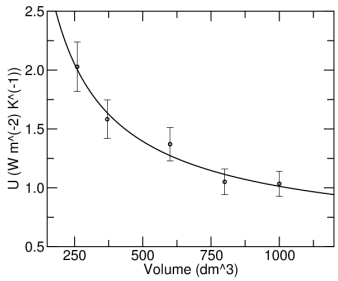

(a)

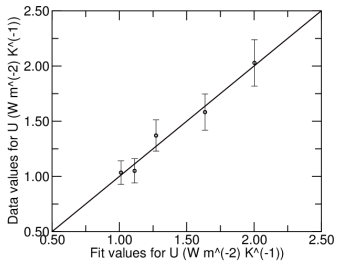

(b)

Figure 5: a) Fitting results of $U_{IT} = V_{IT}^{b} + c$ with calculated U values and b) fit residuals from LAPESA Inertial Tank's data

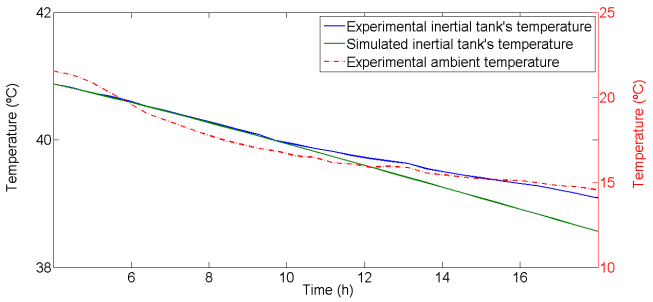

(a)

Figure 6: Simulink implementation of Inertial Tank heat transfer coefficient U_{IT} validation and b) its results in comparison with the tank's experimental change in temperature over time

the other hand, scenario S2, has no area limitations but the excessive electrical energy generated is lost.

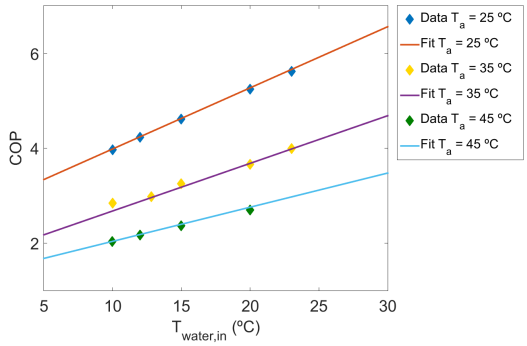

(a)

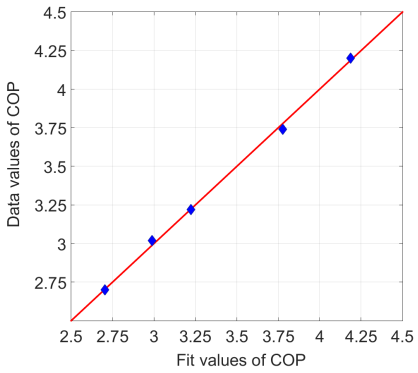

(b)

Figure 7: a) Fitting results for calculated EER values as a function of the water's entering temperature at the chiller and b) fitting residuals for $T_a = 35°$

Table II: Two different case studies for the GA optimization

Scenario	Limited area	PV generation sold to grid
S1	30 m^2	Yes
S2	No	No

In the case of S1, the optimization converges after 21 generations totalizing 3.7 days running. The stopping criteria was defined to be a number of stalled generations between a best fitness value change of 10^{-6}. This number was set to be 5 in both cases, since this optimization running time is extremely high. The best and

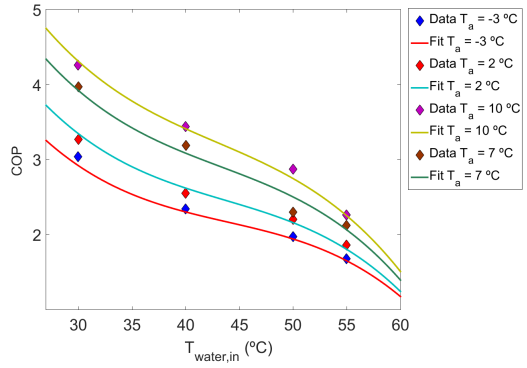

(a)

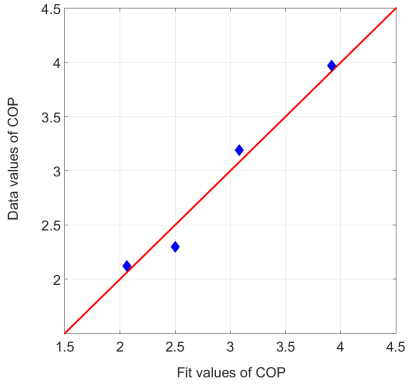

(b)

Figure 8: Fitting results for calculated COP values as a function of the water's entering temperature at the heat pump

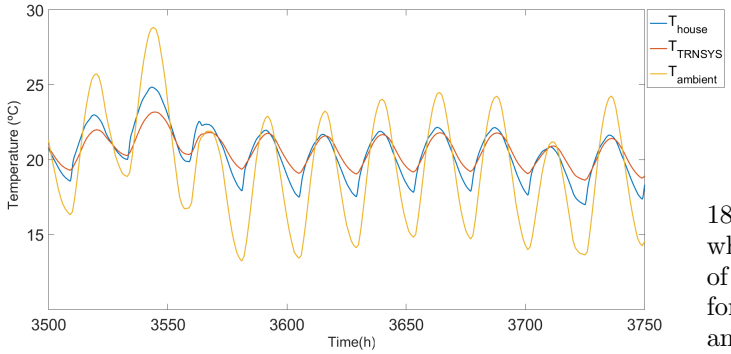

Figure 9: Detailed comparison of the house's room temperature change between the TRNSYS and SIMULINK implementation over a specific summertime period.

mean fitness values were 37192.3 EUR and 37023.8 EUR, respectively. The optimization process took 4.3 days and at the 20th generation, the S2 optimization determined a best and mean fitness values of 40889.3 and 40913.5 EUR, respectively.

The parameters have to be in accordance with the available components on the market and their properties. Therefore there was the need to apply the S1 and S2 optimal solutions to a real case scenario replacing the values for their practical correspondences. Table III displays the chosen system's parameters that make the lowest system's costs going from the tanks' catalog volume to the number of PV and PVT modules. As mentioned the implemented PVT module has an area of 1.42 m^2 while the typical PV module is 1.6 m^2.

Taking the optimal solution of S1, the remaining components of the system will be analyzed throughout the next section.

$$[I_n] = [A_{PVT} \;\; A_{PV} \;\; V_{DHW} \;\; V_{IT} \;\; T_{DHWset,2} \;\; T_{ITset,w} \;\; T_{ITset,s}]$$

Figure 10: System's input variables that make up an individual's, I_n, genetic code for GA optimization

Table III: GA Optimization parameters for a real case scenario, replacing the optimized values with the available components on the market

Scenario	A_{PVT} (m^2)	A_{PV} (m^2)	V_{DHW} (m^3)	V_{IT} (m^3)
S1	7.100	22.4	0.366	0.370
S2	7.100	16	0.366	0.370

Scenario	$T_{DHW,set,2}$ (°C)	$T_{ITset,w}$ (°C)	$T_{ITset,s}$ (°C)
S1	43	35	11
S2	43	35	11

Scenario	Costs (EUR)
S1	37551.9
S1	40761.9

A. PV+PVT+DHW

The winter and summertime generate 3776.6 kWh and 1890.5 kWh, respectively, totalizing 5667.1 kWh for the whole year. The PV electricity generation covers 53.7 % of the demand, being the climatization block responsible for 34 % of it. The maximum η_{el} reached for both PV and PVT was 11.9 % and 10.5 %, respectively.

Figure 11-a) details the relationship between η_{th} and the PVT thermal performance. Around 1813 h, G_T reaches a maximum of 1041.7 W/m^2 and T_a = 25 °C, leading to a 7.15 °C difference between T_{fo} and T_{fi}. The maximum η_{th} for the whole year is 39 %. Figure 11-b) shows a detailed view for a DHW weekly consumption. The four events of the washing machine usage at the weekends are distinguishable from its higher extraction flow rate, m_{extr}, when comparing with the daily shower usage. Although T_{DHW} goes below 40 °C a considerable number of times, no showers occur below that temperature, being the washing machine usage, on days with a low incident irradiance, the cause of that. The PVT modules cover 78.2 % of household's total DHW demand, with 3253.7 kWh of thermal output.

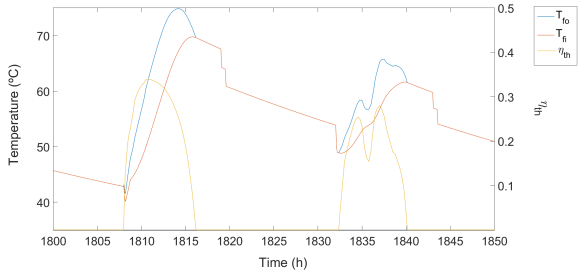

(a)

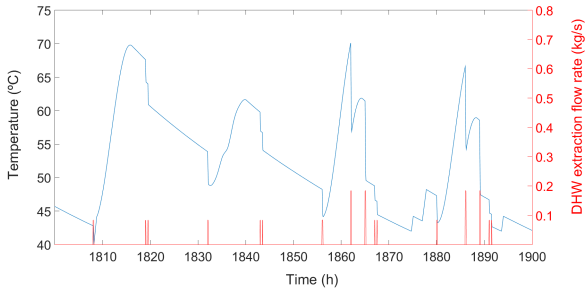

(b)

Figure 11: a) Detailed view, from the S1 optimization, of the entering, T_{fi}, and exiting, T_{fo}, water temperatures (left yy axis) and thermal efficiency, η_{th} (right yy axis), of the PVT array, b) detailed view for a specific DHW weekly consumption comparing T_{DHW} (left yy axis) with the DHW extraction flow rate, $\dot{m}_{extr}$, (right yy axis).

B. Climatization Block

Figure 12-a) plots the annual room and ambient temperature variation. The room's setpoint for the winter and summertime period is 20 °C and 22 °C, respectively.Although T_{room} goes below 16 °C during certain periods of time, specially for the last and first days of the year, since those periods do not last more than 3 days and at any moment T_{room} goes above 26 °C , the system does not fail once, confirming the S1 optimization result as a valid solution. The annual heating and cooling demand for the building is, then, 11046.9 kWh and 1163.6 kWh, respectively.

C. Financial Analysis

The Net Present Value (NPV) and Levelized Cost of Energy (LCoE) were determined for each optimization scenario. The results are visible in Table IV. The discount rate, dr, was set to be 6.5 % from [9]. The Solar Savings were determined from a system in which the DHW volume was $V_{DHW} = 0.186$ m^3, with a setpoint temperature, $T_{DHWset,2} = 55$ °C, and the investment value relies over the PV+PVT+DHW block. Figure 13 plots the NPV as a function of time and the Payback time is determined when NPV = 0.

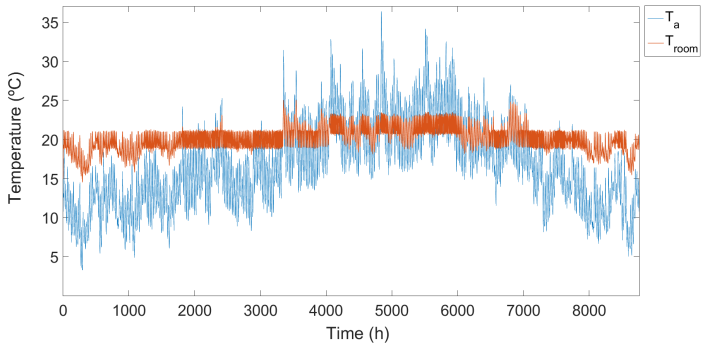

(a)

Figure 12: House room temperature, T_{room}, and ambient temperature, T_a, during a year from S1 optimization

Table IV: Determined investment costs, C_0, the annual balanced electricity costs, C_E, Solar Savings, LCoE and Payback Time for a PV+PVT+DHW investment for both optimization scenarios.

Scenario	C_0 (EUR)	C_E (EUR)	Solar Savings (EUR)
S1	7533	1269.9	1247.4
S2	6765	1476.5	1040.8

Scenario	LCoE (EUR/kWh)	Payback time (years)
S1	0.136	7.9
S2	0.148	8.7

VII. CONCLUSIONS AND FUTURE WORK

The system's components validation through experimental or available data in addition to the GA implementation, demonstrated that despite being a a valid tool to determine the possible optimal system's parameters being, this model is severely constrained by its computation time. This prevents the GA from searching extensively over the solutions space. Since the optimization is constrained to a low number of iterations, it would have been an interesting option to decrease the crossover fraction,

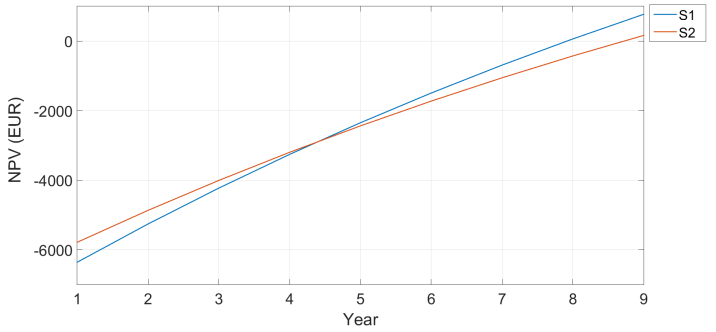

Figure 13: Net Present Value variation (NPV) as a function of time for S1 and S2 optimization. The Payback time happens at NPV = 0

forcing the optimization process to be more volatile or unpredictable, thus, hopefully, increasing the chances of finding a global minimum. It's, however, highly likely that the presented solutions for both case studies are in the near-optimal region.

According to [21], between the 1st of October and the 31st of May , the heating demand for a house with this construction and location is 7544 kWh, corresponding to an average of 30.92 kWh/day, 35.9 % lower than the module's estimations. Additionally, according to the same reference, between the 1st of June and the 30th of September, the cooling demand is 8.38 kWh/day, 36.3 % lower than this work's calculations. The underestimation of the house's thermal capacity can be a significant differentiating factor between these values. This certainly decreases the current PV solar fraction, here determined with 53.7 %, while having no impact on the system's thermal solar fraction, with 78 % for the specified domestic hot water consumption profile. The total PV+PVT solar fraction is 60.6 %.

As expected, the possibility to sell excessive generated electricity at the PV modules improves the investment return and the LCoE on a PV+PVT+DHW system with the optimal configuration. The energy demand overestimation for the model's building impacts, nevertheless, the payback time, increasing it. The PVT capacity seems to be independent of the scenario chosen, which is a consequence of the large investment costs for a low electrical efficiency, leading the GA to adjust the PVT capacity solely to the DHW demand. As PVT and PV technology becomes more competitive, their performance can update the model's current correlations and their integration be assessed.

Acknowledgments

The author would like to thank Professor Luís Filipe Mendes, Doutor António Joyce and João Cardoso.

[1] Onovwiona, H. I., & Ugursal, V. I. (2006). Residential cogeneration systems: review of the current technology. *Renewable and sustainable energy reviews*, 10(5), 389-431.

[2] Dong, L., Liu, H., & Riffat, S. (2009). Development of small-scale and micro-scale biomass-fuelled CHP systems–A literature review. *Applied thermal engineering*, 29(11), 2119-2126.

[3] Zheng, X. F., Liu, C. X., Boukhanouf, R., Yan, Y. Y., & Li, W. Z. (2014). Experimental study of a domestic thermoelectric cogeneration system. *Applied Thermal Engineering*, 62(1), 69-79.

[4] Friedlingstein, P., Andrew, R. M., Rogelj, J., Peters, G. P., Canadell, J. G., Knutti, R., ... & Le Quéré, C. (2014). Persistent growth of CO2 emissions and implications for reaching climate targets. *Nature geoscience*, 7(10), 709.

[5] Radziemska, E. (2003). The effect of temperature on the power drop in crystalline silicon solar cells. *Renewable Energy*, 28(1), 1-12.

[6] Royne, A., Dey, C. J., & Mills, D. R. (2005). Cooling of photovoltaic cells under concentrated illumination: a critical review. *Solar energy materials and solar cells*, 86(4), 451-483.

[7] Dupeyrat, P., Ménézo, C., & Fortuin, S. (2014). Study of the thermal and electrical performances of PVT solar hot water system. *Energy and Buildings*, 68, 751-755.

[8] Tonui, J. K., & Tripanagnostopoulos, Y. (2007). Improved PV/T solar collectors with heat extraction by forced or natural air circulation. *Renewable energy*, 32(4), 623-637.

[9] Kalogirou, S. A., & Tripanagnostopoulos, Y. (2006). Hybrid PV/T solar systems for domestic hot water and electricity production. *Energy conversion and management*, 47(18), 3368-3382.

[10] Axaopoulos, P. J., & Fylladitakis, E. D. (2013). Performance and economic evaluation of a hybrid photovoltaic/thermal solar system for residential applications. *Energy and Buildings*, 65, 488-496.

[11] Agrawal, S., & Tiwari, G. N. (2011). Energy and exergy analysis of hybrid micro-channel photovoltaic thermal module. *Solar Energy*, 85(2), 356-370.

[12] Kim, J. H., & Kim, J. T. (2012). Comparison of electrical and thermal performances of glazed and unglazed PVT collectors. *International Journal of Photoenergy*, 2012.

[13] Ross Jr, R. G. (1980). Flat-plate photovoltaic array design optimization. In *14th Photovoltaic Specialists Conference* (pp. 1126-1132).

[14] García, M. A., & Balenzategui, J. L. (2004). Estimation of photovoltaic module yearly temperature and performance based on nominal operation cell temperature calculations.*Renewable energy*, 29(12), 1997-2010. ISO 690

[15] Skoplaki, E., & Palyvos, J. A. (2009). On the temperature dependence of photovoltaic module electrical performance: A review of efficiency/power correlations. *Solar energy*, 83(5), 614-624.

[16] Perez, R., Ineichen, P., Seals, R., Michalsky, J., & Stewart, R. (1990). Modeling daylight availability and irradiance components from direct and global irradiance. *Solar energy*, 44(5), 271-289.

[17] Erbs, D. G., Klein, S. A., & Duffie, J. A. (1982). Estimation of the diffuse radiation fraction for hourly, daily and monthly-average global radiation. Solar energy, 28(4), 293-302.

[18] Sonntag, R. E., Borgnakke, C., Van Wylen, G. J., & Van Wyk, S. (2009). *Fundamentals of thermodynamics*. 7th Edition. John Wiley & Sons.

[19] Rahman, A., Smith, A. D., & Fumo, N. (2016). Performance modeling and parametric study of a stratified water thermal storage tank. *Applied Thermal Engineering*, 100, 668-679.

[20] Vasconcelos de Paiva, J. A., & Pina dos Santos, C. A. (1990). Coeficientes de transmissão térmica de elementos da envolvente dos edifícios (ITE 28). *Laboratório Nacional de Engenharia Civil*.

[21] Mendes, J. C., Guerreiro, M. R., Pina dos Santos, C. A. & Vasconcelos de Paiva, J. A. (1989). Temperaturas exteriores de projecto e números de graus-dias. *INMG*.